Photoionization Dynamics of Glycine: The First 10 Picoseconds

Dorit Shemesh,[†] Galina M. Chaban,[‡] and R. Benny Gerber*[,†,§]

Department of Physical Chemistry and the Fritz Haber Research Center, The Hebrew University, Jerusalem 91904, Israel, NASA Ames Research Center, Mail Stop T27B-1, Moffett Field, California 94035, and Department of Chemistry, University of California−Irvine, Irvine, California 92697

Received: May 5, 2004; In Final Form: August 27, 2004

Single photon ionization dynamics of glycine is studied by classical trajectory simulations using the semiempirical PM3 potential surface in "on the fly" calculations. The glycine conformer is assumed to be in the vibrational ground state prior to ionization. Initial conditions for the trajectories are weighted according to the Wigner distribution function computed for that state. Vertical ionization in the spirit of the classical Franck−Condon principle is assumed. The main findings are as follows: (1) The photoionization triggers a fast internal rotation about the C−C bond, with the NH_2 group rotating in one direction, and the COOH group rotating in the opposite direction. For the trajectories where the fast rotation occurs, it persists till the end of the simulation (10 ps). The yield for this process is about 6%, suggesting it may be experimentally observable. (2) For many of the trajectories, the photoproduced glycine ion exhibits "hops" between two conformer structures. The rates computed from the dynamics for these conformational transitions differ considerably from RRK predictions. (3) Different behavior of vibrational energy flow is found for different types of modes. There is no significant approach to statistical distribution of the energy throughout the first 10 picoseconds. (4) The preferred dissociation channel is the C−C bond cleavage. Indeed, fragmentation is observed for a few trajectories, one of them shows H atom hopping from the amino group to the carbonyl group prior to dissociation. Another trajectory shows only this hydrogen transfer and the transfer back. Possible experimental implications of some of the findings are briefly discussed.

I. Introduction

The mechanism and dynamics of photoionization of biological molecules are of considerable intrinsic interest and may have potential applications, especially in mass spectrometry. Ionization, carried out by several possible processes,[1−4] is obviously a central aspect of mass spectrometry. At the same time, mass spectrometry has already developed into a major tool in the study and characterization of biological molecules, from small to very large.[5−23] Little is currently known on the dynamical processes that take place upon photoionization of biological molecules. The present article aims at exploring this topic. We chose to focus on single-photon ionization in this first study, since this is probably the conceptually simplest ionization process. It should be recognized, however, that two- and higher order photon ionization are far more common in practice. Glycine is adopted here as a prototypical example, being the smallest amino acid. There is a wealth of relevant data on (neutral) glycine, including the structure of its conformers and their spectroscopy,[24−33] and many characteristics of the potential energy surface. On the contrary, relatively little is known on the glycine ion produced in the photoionization. In particular less is known about the ionic potential energy surface.[34−37] Yu et al.[35] found two ionic conformers at the G2(MP2) level of ab initio electronic structure theory. Both are similar in structure with neutral conformers. The positive charge in both conformers is located on the nitrogen. One ionic conformer has one hydrogen bonding interaction between one hydrogen of the NH_2 group and the carbonyl oxygen. The hydrogens connected to the nitrogen are in the same plane as the C−C═O backbone. The second conformer has a bifurcated interaction linking the amino hydrogens to the hydroxyl oxygen lone pairs. The energy difference between these two isomers at the G2(MP2) level is predicted to be 5.9 kJ/mol. According to the work of Rodríguez-Santiago et al.[36] (DFT and MP2 calculations) there is a third ionic conformer which is similar in structure with another neutral conformer. This conformer has an interaction linking the hydroxyl hydrogen to the amino lone pair.

The channels that open up upon ionization of glycine include the following: internal flow and redistribution of the vibrational energy between the modes; conformational transition of the nascent ion; transfer of hydrogen within the ion;[36,37] fragmentation of the ion.[21,34,37] The study presented here focuses mostly on the first two types of processes: intramolecular vibrational energy redistribution (IVR) and transitions between different conformers. These are believed to be the fastest and most efficient dynamical processes in such systems. However, also chemical processes which involve bond breaking or shifting and require much longer time scales depend ultimately on the outcome of the IVR and conformational transition events. It is important to know whether a statistical distribution of vibrational energy is indeed obtained and on which time scale it is reached. The question is, how long after the ionization a vibrational distribution compatible with RRKM is obtained. The time scale that will be explored here is short, only 10 picoseconds, but it is useful to know if a significant move in the direction of statistical distribution can already be noted. If not, characterization of the patterns of vibrational energy flow is of considerable

* To whom correspondence should be addressed. E-mail: benny@fh.huji.ac.il.
[†] The Hebrew University.
[‡] NASA Ames Research Center.
[§] University of California, Irvine.

10.1021/jp040331o CCC: $27.50
Published on Web 12/07/2004

interest. The issue of conformational transitions is likewise important: Which conformers are populated following ionization, and on which time scale does this take place? This issue is often discussed qualitatively in mass spectrometry, but it seems that it was not studied quantitatively, by dynamics simulations. Another interesting question is whether *some* fragmentation events can take place already on the short 10 ps time scale studied here. Clearly, the yield for such processes on this short time scale is expected to be very low, but it is interesting to explore if the event is not too rare to be seen for some of the trajectories in the set (and hopefully be measured experimentally). It will indeed be seen that for the set of trajectories used, some fragmentation events are found. In summary, the present paper explores the dynamical evolution of the system after ionization, using classical trajectory simulations and a semiempirical potential surface, the choice of which will be discussed later. The structure of the article is as follows. Section II presents the methodology used. In section III, the findings are described and analyzed. Section IV brings concluding remarks.

II. Methodology

A. Potential Energy Surface. Biological molecules are often studied using empirical force fields such as AMBER,[38] OPLS,[39] MMFF94.[40] The advantages of these force fields are that they are simple to use, computationally fast and give adequate results for neutral molecules. However, these force fields do not give reliable description for ionic systems.

A more accurate approach is to use ab initio potentials, but these are computationally expensive, especially for large biological molecules. In dynamical simulations the potential energy is evaluated thousands of times along the trajectories. This step is the main computational effort in this case, and using ab initio potentials would be very time-consuming. Such ab initio simulations would be limited to only very short timescales.

Therefore, we use in this study PM3 semiempirical electronic structure theory.[41] PM3 is one of several modified semiempirical NDDO approximation (neglect of diatomic differential overlap) methods.[42] Rather than performing a calculation of all of the integrals required in the formation of the Fock matrix, three- and four center integrals are neglected in PM3, and one-center, two-electron integrals are parametrized. Thus, in principle, PM3 is closer to ab initio methods than force fields. Additionally, PM3 has recently been applied to calculations of small proteins.[43−45] It is not known if PM3 possesses the capability of correctly describing bond breaking for radical ions. Another problem that may arise is the Hartree−Fock instability and possible degeneracy for open shell systems. Recently, a method has been developed in our group, which improves PM3 potential energy surface.[33] This method employs a coordinate scaling procedure. The modified PM3 potential has been tested for glycine, alanine and proline by calculating the anharmonic frequencies using the VSCF and CC−VSCF[46,47] method, and comparing them to experimental data. The computed anharmonic frequencies are in very good agreement with spectroscopic experiments for these three amino acids. The simulations presented here were carried out with standard PM3. At the same time are also tested some properties of the potential surface (e.g., the barrier for internal rotation of the glycine ion) against ab initio. This is discussed later.

All calculations have been performed using the electronic structure package GAMESS.[48] One of the lowest lying conformers was optimized using PM3 semiempirical electronic structure theory on the neutral surface. This conformer is not the global minimum, but this is an experimentally and theoretically well characterized conformer. The second derivative (Hessian) matrix was calculated to ensure that the stationary point is indeed a minimum (all eigenvalues are positive). Harmonic normal-mode analysis was performed on this geometry. Initial coordinates were chosen by the following procedure: Each mode has been distorted from equilibrium. For each mode, 16 different positions were chosen and the Wigner distribution for these geometries was calculated. By this procedure, 384 initial geometries were found.

For each geometry in the Franck−Condon regime, single-photon ionization was modeled by vertical promotion into the ionic potential energy surface. Afterward the trajectory was propagated in time on the ionic PM3 potential energy surface (using ROHF in the Hartree−Fock part of the code). Trajectories, where the ROHF energy calculations failed to converge, or for which energy conservation was not satisfied were rejected. Energy was considered to be conserved when the difference between the initial total energy and the total energy (in atomic units) at the current time step was smaller than 5×10^{-5}. The analysis was all carried out for the remaining 361 trajectories. Note that the ionization model used does not correspond to a monochromatic source, but to radiation having frequencies across the range of the photoionization (absorption) spectrum. This means that different trajectories had different energies in the ionic state.

B. On-the-Fly Molecular Dynamics Simulation. The method used for the simulation is "on the fly" molecular dynamics[49−55] that is implemented into the electronic structure program package GAMESS.[48] Recently studies of dynamics on the fly using QM/MM and semiempirical potentials have been pursued by Hase[56,57] and co-workers. Obviously, some quantum effects are expected to play a role, and these are neglected in the classical approach. Zero-point energy is probably the most important quantum effect neglected in this study. However, the excess energy is fairly high on the ionic states ($E > 0.8$ eV), and we assume the classical description should be reasonable. In "on the fly" molecular dynamics, at each time step, the current potential energy is evaluated and the forces are computed. The atoms are moved according to these forces to a new position (next time step), and there again, the forces are calculated from the potential energy and the atoms are moved, and so on. A very demanding SCF (ROHF) convergence criterion of 10^{-11} was employed to ensure in this case accurate force calculations for the time scale of the study. The default value of 10^{-5} employed in the standard GAMESS code is too big for the present case. Calculations with this value have shown that the computed trajectory contains unphysical artifacts. The reason is obvious: The more accurate the potential energy calculation, the more accurate will be the force calculations at that point. Fewer errors are then accumulated during the simulation and the calculated trajectory deviates less from the true one. Each trajectory was calculated for 10 ps with a time step of 0.1 fs (to ensure energy conservation).

C. Representation of Initial Conditions. The glycine molecule is assumed to be initially in its vibrational ground state. This is an experimentally realizable (e.g., in low temperature beam experiments), well-defined condition. For such an initial state, the classical description is quite unrealistic (classically, the system at $T = 0$ K is initially at rest at the minimum configuration, with no zero-point energy), so there will be only one classical trajectory for these conditions. Classical description becomes closer to reality if the simulations are done for initial

temperature $T > 0$, in fact for sufficiently high T. In summary, the ground-state vibrational wave function is appropriate for sampling the initial state. Furthermore, for this state, the anharmonic corrections are modest, and a harmonic wave function seems a reasonable wave function.

To sample trajectories according to the initial state we use the Wigner distribution function:[58]

$$W(r,p) = \left(\frac{1}{2\pi\hbar}\right)^N \int \mathrm{d}s \exp\left[\frac{is\cdot p}{\hbar}\right]\cdot\Psi^*\left(r+\frac{s}{2}\right)\Psi\left(r-\frac{s}{2}\right) \quad (1)$$

where ψ is the wave function of the state, r is the coordinate, and p is the momentum.

Each normal mode is treated as a classical harmonic oscillator in its ground vibrational state. Substitution of the harmonic oscillator wave function into the Wigner distribution gives the Wigner distribution for an n-dimensional harmonic oscillator:

$$W(q,p) = (\pi\hbar)^{-n}\prod_{i=1}^{n} \mathrm{e}^{-p_i^2/\alpha_i}\,\mathrm{e}^{-k_i q_i^2/\alpha_i} \quad (2)$$

q_i is the normal mode, and p_i is the corresponding momentum. k_i is the force constant of the ith normal mode and α_i is related to the corresponding vibrational frequency ($\alpha_i = \hbar\omega_i$). For the excitation process, we assume, in the spirit of the Franck−Condon principle, vertical promotion to the ionic state. This implies that the initial velocities are zero on the ionic surface, the configurations being those sampled for the neutral species.

To test the validity of the statistical approximation for the interconversion between conformers, the results of the trajectory calculations will be compared with the classical RRK rates. For a process at energy E, the RRK rate is given by[59]

$$k(E) = A\left(\frac{E-E_0}{E}\right)^{s-1} \quad (3)$$

where A is taken as

$$A = \left(\frac{\prod_{j=1}^{s}\upsilon_j}{\prod_{i=1}^{s-1}\upsilon_i}\right) \quad (4)$$

E is the total energy, E_0 is the energy barrier, and s is the number of degrees of freedom, in this case 24. υ_j is the frequency from the initial minimum geometry and υ_i is the frequency from the transition state. The transition state of the interconversion between conformers was found by searching for an extremum along the reaction path, and checking for a configuration having a single negative Hessian frequency eigenvalue. If the initial state corresponds to a distribution of energies of the molecules rather than to be a monoenergetic ensemble, the overall RRK rate is

$$\bar{k}_{\mathrm{RRK}} = \int_{E_0}^{\infty} P(E)A\left(\frac{E-E_0}{E}\right)^{s-1}\mathrm{d}E \quad (5)$$

where $P(E)\,\mathrm{d}E$ is the fraction of initial states having energies between E and $E + \mathrm{d}E$. In the statistical approximation, the specific initial conditions for an ensemble are assumed to be "forgotten" on a very short time scale. Thus, $P(E)$ in eq 5 represents the only effect of a nonmonoenergetic ensemble on the RRK reaction rate. The validity of RRK does not, of course, depend on having a monoenergetic ensemble, and can be tested in principle for any ensemble.

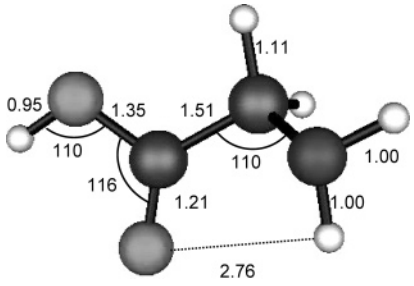

Figure 1. Global minimum of glycine calculated by PM3. Bond lengths are in angstrom, and angles are in degrees.

Another way of calculating the rate constant is to use the microcanonical transition state theory (i.e., RRKM theory), wherein the rate constant for a monoenergetic initial state ensemble is given by[59]

$$k(E) = \frac{N^{\mathrm{TS}}(E-E_0)}{h\rho(E)} \quad (6)$$

with $N^{\mathrm{TS}}(E - E_0)$ being the number of states in the transition state and $\rho(E)$ the reactant density of states. This includes static quantum effects. We chose to use the RRK rate constant, since it compares better with the results of classical dynamics performed in this study.

III. Results and Discussion

III.a. Initial State. The initial state was taken to be one of the lowest lying conformers of glycine. Figure 1 shows the PM3 geometry of this state. The most stable conformer differs from this geometry by the configuration of the NH_2 group. The most stable conformer has C_s symmetry; the two amino hydrogens interact with the carbonyl oxygen. For the conformer chosen here, the bond lengths at the PM3 level deviate only by up to 0.01 Å and the angles by 1° compared to the ab initio MP2/TZP level. One notable difference is the length of the hydrogen bond between the NH and the CO group: PM3 predicts a bond length of 2.76 Å, whereas MP2/DZP predicts a shorter length of 2.69 Å. There are also some differences (up to 2°) in the torsion angles. Only the N−C−C−O(H) angle differs significantly. PM3 predicts 127°, whereas MP2/DZP predicts 138°. It can be concluded, that this glycine conformer is well described by PM3. The neutral geometry can be characterized by an almost planar arrangement of the C−COOH group and by a pyramidal arrangement of the C−NH_2 part of the molecule. The nitrogen is sticking out of the plane, whereas the hydrogens connected to it point into the plane. The most similar ionic minimum differs mainly in the arrangement of the NH_2 group. The nitrogen in the ionic conformer is lying in the plane of the C−COOH part of the molecule. All of the hydrogens except the hydroxylic one lie now perpendicular to the molecular plane described above.

The initial mean charge immediately after the ionization is located for all of the trajectories sampled mainly on the nitrogen (70%). The lone pair of the nitrogen has the lowest ionization potential in the molecule. This is also confirmed by experiment.[21] The ionization potential calculated by PM3 is 8.9 eV. This agrees well with previous experiments and theoretical work.[21,35−37] Theoretical calculations predict an ionization potential between 8.8 and 9.2 eV depending on the level of theory used. The experimental works give an ionization potential between 8.8 and 8.9 eV.

III.b. Onset of a Rotary Motor-Like Behavior. Thirty-seven trajectories out of 361 show this fast internal rotation. The

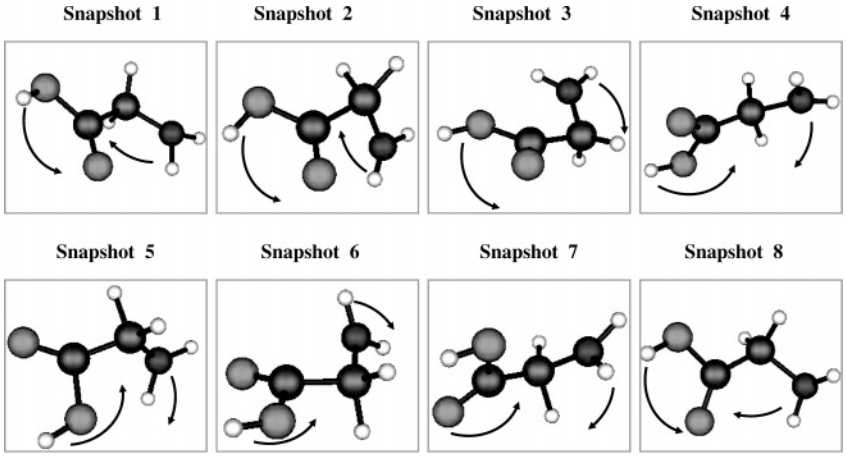

Figure 2. Snapshot of one whole rotation. The COOH group is rotating in one direction, and the NH_2-CH_2 group is rotating into the opposite direction. The axis of rotation is the C−C bond.

statistical weight of these events from the Wigner distribution is 5.86%. One trajectory is chosen here in order to illustrate the mechanism of the rotation. In this trajectory the NH_2 antisymmetric stretch was initially distorted from equilibrium. The mass-weighted normal mode coordinate q was set to 23.58 au. Basically this is equal to lengthening one NH bond from 1.00 to 1.21 Å and shortening the second NH bond from 1.00 to 0.78 Å. The system was ionized vertically at this geometry. The potential energy of this geometry on the ionic surface is about 2.68 eV higher than the potential energy of the ionic equilibrium geometry described above. The initial geometry has the NH_2 group pointing out of plane. Modes which involve mainly the NH_2 group are initially strongly excited. These modes are the NH_2 symmetric stretch, NH_2 antisymmetric stretch and the HNH bend. The corresponding frequencies are 3505.39, 3437.05, and 1609.92 cm^{-1}. These modes contain a large part of the initial kinetic energy. During the first 2 ps this energy flows out of these modes and into the rotational mode. The motion in the first 2 ps is characterized by mainly the NH_2 antisymmetric stretch together with the wagging motion of the NH_2 group with respect to the plane of the C−COOH group. On the ionic surface, the nitrogen tends to be in the same plane as the C−COOH group (local minimum, named here conformer I). After 1.86 ps the first rotation starts. The CH_2-NH_2 group is rotating in one direction and the COOH group in the opposite direction. This is due to angular momentum conservation. The rotation is about the C−C bond. This rotation persists until the end of the simulation (10ps). Snapshots of the rotation are drawn in Figure 2. There are a total number of 21 rotations in this time scale. The rotation angle (torsion angle of N5−C3−C2−O1) as a function of time is drawn in Figure 3. The graph is based on discrete points and therefore does not always reach 0° and 180°. The average time for one rotation is 0.28 ps which corresponds to a frequency of 119.13 cm^{-1}. The potential energy barrier for this rotational motion is drawn in Figure 4. The torsion angle depicted here is the torsion angle between N5−C3−C2−O1. Initially this torsion angle is equal to −53°. The lowest energy geometry corresponds to the local ionic minimum. The barrier for the rotation in the PM3 calculation is very small (0.11 eV) compared to the excess energy of 2.68 eV available in the system. The barrier calculated with MP2/DZP is higher (0.28 eV), but the qualitative picture is the same. The system still has enough energy to overcome the barrier. It can be expected that the system will show rotation also with the ab initio barrier. There might be less rotation due to the higher barrier. As was pointed out above, in the trajectory discussed here, the system does not start rotating immediately after the

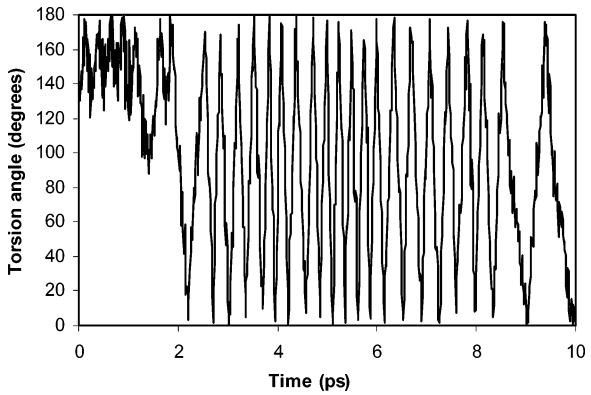

Figure 3. Torsion angle N5−C3−C2−O1 as a function of time for the trajectory that shows the rotation.

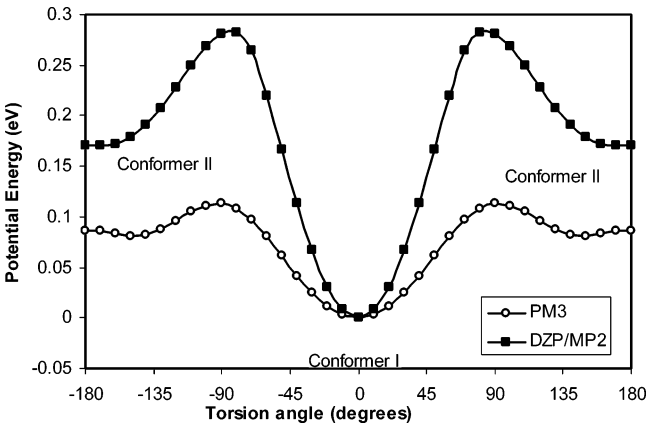

Figure 4. Potential energy as a function of the torsion angle N5−C3−C2−O1 calculated by PM3 and DZP/MP2

ionization. The molecule needs to have enough energy in the rotational mode in order to overcome the barrier. The rotational mode is characterized by the wagging of the NH_2-CH_2 group against the COOH group. The lowest frequency mode of the ionic glycine (70.08 cm^{-1}) has this characteristic. Also, a normal-mode analysis of the transition states in Figure 4 reveals that the imaginary frequency has the same vibrational motion. So this mode can be clearly identified as being responsible for the motion. The energy initially in this mode is indeed not enough to overcome the barrier. It takes about 2 ps for the energy to flow out of the NH_2 modes and into this rotational mode. After 2 ps the energy in this mode exceeds the barrier and the molecule starts to rotate freely. Figure 5 shows the

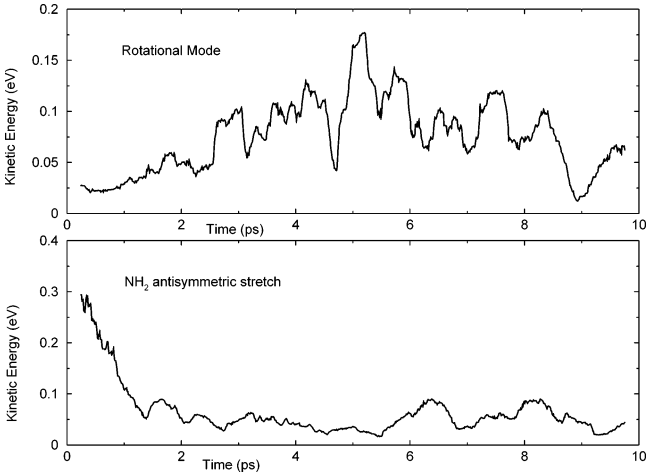

Figure 5. Kinetic energy of the rotational mode and the NH_2 antisymmetric stretch for the trajectory that shows the rotation.

energy in the NH_2 antisymmetric stretch and the energy in the rotational mode as a function of time. The kinetic energy is very noisy; therefore, it is averaged over the period of the slowest vibration, i.e., 0.5 ps in order to get an energy envelope.[60] Another interesting feature of this trajectory is that during the rotation the C−C bond once almost breaks. The C−C bond at 4.8 ps reaches a length of 1.93 Å. The length of the C−C bond that corresponds to the transition state of dissociation on the PM3 ionic potential surface is predicted to be 2.01 Å. This trajectory also shows at several points the rotation of the NH_2 group about the N−C bond. The two hydrogens connected to the nitrogen interchange during this rotation. The computed yield for fast internal rotation upon photoionization is 5.86%. This yield for producing the ultrafast rotation upon excitation should suffice to make experimental detection of the effect feasible. Finally, the fast internal rotation is expected to decay ultimately, due to energy flow into other modes. However, the rotation evidently persists at least for 10 ps, the duration of the present simulation.

III.c. Conformational Transition and the Validity of RRK. There are also trajectories where the system overcomes the barrier for the rotation, but above the minima loses again the excess energy and stays in one of the two flat minima of Figure 4. The barrier between these two minima is very low, so that one cannot separate them as two different conformers. Therefore, we refer to both as conformer II. Conformer II can be obtained from conformer I by rotating the COOH group by 180° about the C−C bond. In these cases, the trajectory shows hopping between two conformers on the ionic surface. The hopping between conformers is similar to that shown in a simulation of torsional isomerization in a tetraatomic system by Schranz and Collins.[61] A total of 133 trajectories out of 361 show this hopping. The statistical weight for this event is 30.27%. Some trajectories show only hopping between one conformer and the other. Some trajectories show a few hopping events back and forth before the molecule settles for a while in the other conformer structure. One example of hopping is shown in Figure 6. The mode that is displaced initially from equilibrium has a frequency of 1246.41 cm^{-1} and involves motion of the CH_2 and OH groups. The initial displacement is 10.63 au. Here the first hopping occurs at 2 ps. The molecule stays in conformer II for about 3 ps before it jumps back to the first conformer for another 0.5 ps. Finally it jumps again to conformer II. Figure 7 shows the first hopping time (calculated from the RRK rate of this process) as a function of the excess energy. The excess energy is the difference between the potential energy at the ionic

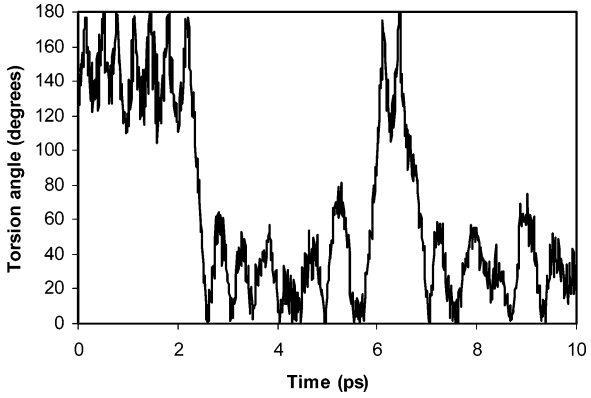

Figure 6. Torsion angle N5−C3−C2−O1 as a function of time for one of the trajectory that shows hopping between the conformers.

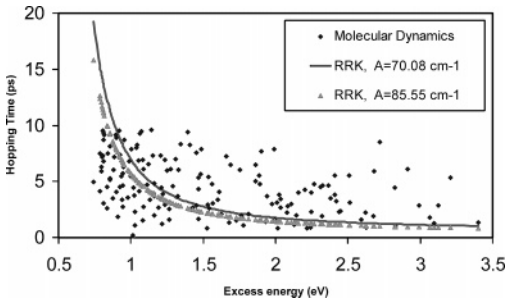

Figure 7. First hopping time as a function of the excess energy available. The upper graph is received from molecular dynamics, whereas the lower graph is calculated by RRK.

TABLE 1: Frequencies in cm^{-1} for the Ionic Ground State and the Transition State

ionic ground state	transition state	ionic ground state	transition state
70.08	60.63i	1126.01	1113.25
199.21	168.55	1246.41	1263.93
274.18	279.17	1286.96	1273.4
432.49	382.78	1324.6	1334.55
511.63	474.09	1464.24	1434.86
525.45	519.4	1609.92	1613.97
549.69	680.32	1967.95	1991.88
798.46	779.92	2817.65	2814.2
868.98	862.92	2912.52	2905.03
905.82	897.76	3437.05	3472.19
1017.9	993.79	3505.39	3514.33
1045.46	1052.03		

The Imaginary frequency is denoted by i.

surface after ionization and the ionic local minimum described above. The RRK results are compared with the hopping rates computed directly from the trajectories. Note that different trajectories correspond in general to different excess energies, depending on the initial geometry for which the trajectory was sampled. Two RRK lifetimes are plotted. One uses $A = 70.08$ cm^{-1}. The vibrational motion related to this frequency has been shown to be responsible for the hopping (and rotation). The lower lying RRK graph uses the ratio between the frequencies as in eq 4, which is here equal to 85.55 cm^{-1}. The frequencies used are tabulated in Table 1. It seems from Figure 7 that the dynamics results differ qualitative from RRK. Note that we are testing RRK here for a nonmonoenergetic ensemble. At any "slice" of energy E, $E - \Delta E \leq E \leq E + \Delta E$ where ΔE is small, the results can be compared with the monoenergetic RRK expression. In the ensemble used, we have few trajectories for each energy E, but on the other hand, there are results for many E values so the test of RRK here is quite stringent. Some

trajectories show faster hopping times, some slower hopping times as predicted by RRK. RRK assumes statistical distribution of the vibrational energy, which is not the case here, at the short time scales investigated. This is due to different coupling strengths between the modes. Modes that are strongly coupled to the rotational degree of freedom show faster hopping times than predicted by RRK and vice versa. Also the process takes place in highly nonequilibrium conditions and the trajectories do not follow the minimum energy path between the conformers. Whether hopping occurs or not, does not seem to depend significantly on the excess energy available which is central to RRK. The minimum excess energy in these trajectories is 0.8 eV for some trajectories. Among them, some show hopping and some do not. This seems to depend on how strongly coupled the initially excited mode is with the rotational mode. It should be noted that a quantitative, rigorous way to show if the system is statistical or not is to work with an ensemble of trajectories with constant energy and to draw the lifetime probability distribution for this ensemble from the RRK model, i.e.

$$P(t) = k(E)\, \mathrm{e}^{-k(E)t} \tag{7}$$

where $k(E)$ is the RRK rate and t is the time. This lifetime probability should then be compared to the lifetime probability obtained from molecular dynamics.[62] It seems, however, that the rates from the trajectories fluctuate so extremely from the RRK rates, that qualitatively the behavior is very non RRK-like.

III.d. Energy Flow between Normal Modes. It is often assumed that IVR takes place in the time scale of several picoseconds. In terms of temperature, the normal modes should equilibrate in this time scale to a common temperature. The normal modes of the equilibrium structure of the ionic global minimum most similar to the neutral lowest energy conformer were calculated. These modes were used in order to analyze the energy partition into normal modes during the simulation. It should be noted that the normal mode approximation fails for large displacements from equilibrium. The mean energy partition into the normal modes was calculated using all 361 trajectories with their statistical weights obtained from the Wigner distribution.

The kinetic energy of each mode in each trajectory is calculated during the dynamics and averaged using the Wigner distribution. From the average kinetic energy in each mode, the temperature of each mode is obtained. The temperature of each mode at time t is therefore defined by

$$T(t) = \sum_i \frac{2w_i E^i_{\mathrm{kin}}(t)}{k} \tag{8}$$

where the sum is over all trajectories sampled, w_i is the statistical weight of trajectory i, k is the Boltzmann factor, and $E^i_{\mathrm{kin}}(t)$ is the kinetic energy of trajectory i at time t.

The fluctuations of the temperature have a high frequency, and were smoothed with respect to time variation. The temperatures so obtained are referred to as effective temperatures. Figure 8 shows the effective temperature of four modes as a function of time. These modes were selected out of the set of 24 modes in order to show how different frequencies and different locations of the normal modes affect the energy flow between the modes.

Two of them correspond to the NH_2 group. These modes are the NH_2 bending (frequency: 1609.92 cm^{-1}) and the NH_2 rocking mode (frequency: 868.98 cm^{-1}). Another mode depicted here is a skeletal movement mode (432.49 cm^{-1}). The last mode chosen is the OH stretch (3815 cm^{-1}). The OH stretch has the highest frequency in the molecule. No other modes involve vibration of this group to this large extent. Because of the high frequency and the location of this mode, it is isolated from other modes and does not participate effectively in the energy flow. The temperature of this mode remains almost constant during the 10 ps of simulation. The other modes are more excited than the OH stretch. The NH_2 bending mode and the NH_2 rocking mode are in the same part of the molecule, and also their frequencies have a ratio of almost 1:2. Therefore, between these two modes, the equilibration is faster and takes about a few picoseconds. The skeletal movement mainly involves the heavy atoms. It almost reaches equilibration with the NH_2 modes in the time scale of 10 ps. The frequency of this mode is almost half the frequency of the NH_2 rocking mode which also helps with the energy flow.

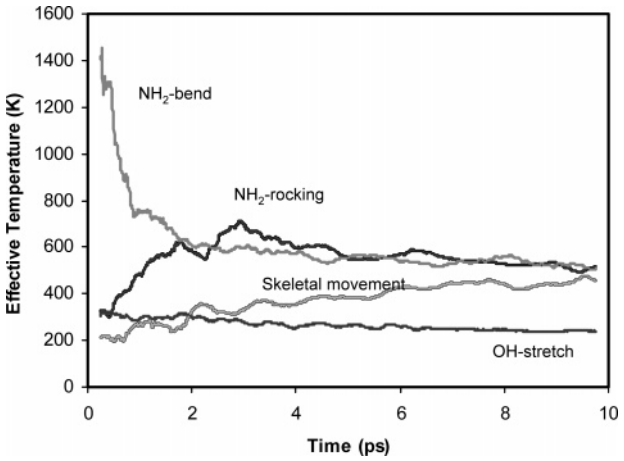

Figure 8. Effective temperature of four normal modes of glycine as a function of time.

It can therefore be concluded that the time scale of equilibration between all of the modes in this system is definitely longer than 10 ps. Although RRKM is a very well established theory,[59,62−66] there exist cases where some of the assumptions break down.[67−81] The system under study clearly does not show fast IVR. The efficiency of the energy flow between two modes depends on two parameters: the geometric proximity of the modes and the ratio between their frequencies. The geometric location of the modes has a stronger influence on the efficiency of the energy flow. When modes have the same location within the molecule, energy flow between them is fast. A low-order resonance can also strongly couple the modes, but this depends on the mismatch of frequencies. In the present example, the strength of the coupling between modes is most strongly dependent on geometry.

III.e. Fragmentation of Glycine. The lowest barrier for fragmentation calculated by Simon et al.[37] corresponds to the cleavage of the C−C bond. The predicted values lie between 0.7 to 0.84 eV depending on the method used (DFT or CCSD-(T)) and whether zero-point energy is included or not. Figure 9 shows the potential energy barrier for the glycine ion as predicted by PM3. The barrier height is 0.93 eV which is close to above calculated values. The barrier lies at the C−C distance of 2.01 Å. Fragmentation is observed in two of the trajectories calculated. The statistical weight for this event is about 0.15%. Table 2 shows the expected fragmentation time calculated from the RRK rate as a function of the excess energy. Table 3 shows frequencies used for calculating the preexponential factor A in

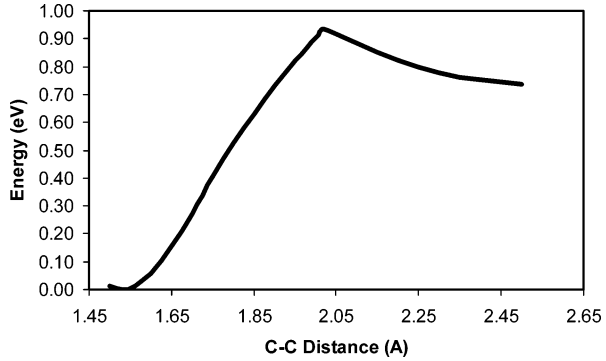

Figure 9. Potential energy along the C−C bond.

TABLE 2: RRK Lifetime for Fragmentation for Different Excess Energies

excess energy (eV)	lifetime (s)	excess energy (eV)	lifetime (s)
1.4	2.64×10^{-4}	2.8	5.10×10^{-11}
1.6	1.89×10^{-6}	3	2.44×10^{-11}
1.8	7.53×10^{-8}	3.2	1.30×10^{-11}
2	7.64×10^{-9}	3.4	7.59×10^{-12}
2.2	1.37×10^{-9}	3.8	3.14×10^{-12}
2.4	3.61×10^{-10}	4.6	9.06×10^{-13}
2.6	1.23×10^{-10}	5.6	3.32×10^{-13}

TABLE 3: Frequencies in cm^{-1} for the Initial State and the Transition State[a]

initial state	transition state	initial state	transition state
56.64	1176.33i	1171.25	1135.41
266.23	34.02	1213.07	1184.9
343.21	205.65	1244.01	1228.3
381.52	290.67	1286.40	1355.58
471.50	359.87	1452.42	1432.54
501.95	381.06	1606.50	1639.9
635.08	448.28	1952.48	2081.88
817.79	498.72	2910.82	2973.3
871.62	720.45	2983.06	3003.87
964.02	850.76	3325.10	3455.79
1029.69	864.72	3435.67	3509.39
1064.52	954.15		

[a] The imaginary frequency is denoted by i.

the RRK rate (eq 4). One trajectory that shows fragmentation will be discussed here in detail. In this trajectory, the NH_2 symmetric stretch is distorted to 31.56 au. The excess energy here is 5.5 eV. After 1.13 ps, the distance between the two carbon atoms exceeds 2.01 Å. The distance between these atoms grows further and yields two fragments. The dynamic stops at 1.22 ps due to convergence problems. At this time, the distance between the two fragments is 4.49 Å. The RRK fragmentation time predicted for excess energy of 5.5 eV is 0.36 ps. The dynamic gives a value about four times higher. Since only a few trajectories undergo fragmentation during the first 10 ps, the statistics is insufficient for conclusions. However, the tentative evidence suggests that RRKM underestimates the fragmentation time for these events.

III.f. Hydrogen Transfer. One of the trajectories shows proton transfer. The mode with the frequency of 213.97 cm^{-1} was here distorted to 111.03 au. In this trajectory one of the hydrogens connected to the nitrogen jumps at 0.32 ps to the oxygen of the carbonyl group, stays there until 1.32 ps, and jumps back again. The excess energy is in this case 3.9 eV. In another trajectory there is first a hydrogen transfer and then the fragmentation occurs. The initial condition for this trajectory is distortion of the normal mode of the NH_2 antisymmetric stretch to a value of 32.16 au.

IV. Concluding Remarks

The photoionization process of glycine is simulated using "on the fly" molecular dynamics on the PM3 potential energy surface. The photoionization triggers a fast rotation, where the NH_2 group rotates in one direction and the COOH group in the opposite direction. This fast internal rotation begins about 2 ps after ionization, and persists for at least 8 ps. The statistical weight for this event is about 6%. The magnitude of the yield for producing the fast rotor suggests that it should be feasible to observe the effect. This will obviously require an approach using ultrafast spectroscopy. This result also suggest that it may be possible to develop this process as a model system for a photodriven molecular motor. It is of interest to explore the possible occurrence of ultrafast rotation upon photoionization also in related systems. This is currently pursued by the authors. Another interesting feature of this system is the hopping between two conformers on the ionic surface. The hopping lifetimes predicted by RRK differ significantly from the lifetimes observed by Molecular Dynamics. In particular, the dependence of the conformational transition rates on the excess energy from the dynamics differs considerable from RRK. This is related to the interesting issue of statistical behavior and intramolecular vibrational energy redistribution. Some normal modes are found to be weakly coupled here. Complete IVR does not take place on the time scale of 10 ps. The system therefore shows strong nonstatistical behavior. The occurrence of fast transitions between conformers, to an extent invalidating RRK estimates of the transition rates, may be of considerably interest for the dynamics of biological molecules and their structural transitions, a field which is receiving considerable attention at the present time.

Although the mean fragmentation time for this system is expected to be very long, and much beyond our simulation time scale, the excess energy for some of the trajectories sampled were large enough, to the point that fragmentation took place. Statistics for the fragmentation events is insufficient, but tentative evidence points to the rate computed from the dynamics being considerably slower than the RRK rate. The topic of fast fragmentation events within the ionization process seems to us to merit considerable future attention.

Acknowledgment. We thank Dr. M. Schmidt for helpful comments on PM3 in GAMESS. Helpful discussions with Professor C. Lifshitz are gratefully acknowledged. This research was supported under the of the auspices of the Saerree K. And Louis P. Fiedler Chair in Chemistry at the Hebrew University of Jerusalem.

References and Notes

(1) Yamashita, M.; Fenn, J. B. *J. Phys. Chem.* **1984**, *88*, 4451−4459.
(2) Yamashita, M.; Fenn, J. B. *J. Phys. Chem.* **1984**, *88*, 4671−4675.
(3) Alexandrov, M. L.; Gall, L. N.; Krasnov, N. V.; Nikolaev, V. I.; Pavlenko, V. A.; Shkurov, V. A.; et al. *Bioorg. Khim.* **1984**, *10*, 710−712.
(4) Karas, M.; Bachmann, D.; Bahr, U.; Hillenkamp, F. *Int. J. Mass Spectrom. Ion Processes* **1987**, *78*, 53−68.
(5) Bowers, M. T.; Marshall, A. G.; McLafferty, F. W. *J. Phys. Chem.* **1996**, *100*, 12897−12910.
(6) Burlingame, A. L.; Boyd, R. K.; Gaskell, S. J. *Anal. Chem.* **1998**, *70*, 647R−716R.
(7) Chalmers, M. J.; Gaskell, S. J. *Curr. Opin. Biotechnol.* **2000**, *11*, 384−390.
(8) Aebersold, R.; Goodlett, D. R.; *Chem. Rev.* **2001**, *101*, 269−295.
(9) Nyman, T. A. *Biomol. Eng.* **2001**, *18*, 221−227.
(10) Mann, M.; Hendrickson, R. C.; Pandey, A. *Annu. Rev. Biochem.* **2001**, *70*, 437−473.
(11) Griffiths, W. J.; Jonsson, A. P.; Liu, S.; Rai, D. K.; Wang, Y. *Biochem. J.* **2001**, *355*, 545−561.
(12) Jonsson, A. P. *Cell. Mol. Life Sci.* **2001**, *58*, 868−884.

(13) Mano, N.; Goto, J. *Anal. Sci.* **2003**, *19*, 3−14.
(14) Ferguson, P. L.; Smith, R. D. *Annu. Rev. Biophys. Biomol. Struct.* **2003**, *32*, 399−424.
(15) Lin, D.; Tabb, D. L.; Yates, J. R., III. *BBA Proteins Proteom.* **2003**, *1646*, 1−10.
(16) Aebersold, R.; Mann, M. *Nature* **2003**, *422*, 198−207.
(17) Standing, K. G. *Curr. Opin. Struct. Biol.* **2003**, *13*, 595−601.
(18) Köster, C.; Grotemeyer, J. *Org. Mass Spectrosc.* **1992**, *27*, 463−471.
(19) Schlag, E. W.; Grotemeyer, J., Levine, R. D. *Chem. Phys. Lett.* **1992**, *190*, 521−527.
(20) Lockyer, N. P.; Vickermann, J. C. *Int. J. Mass Spectrom.* **1998**, *176*, 77−86.
(21) Vorsa, V.; Kono, T.; Willey, K. F.; Winograd, N. *J. Phys. Chem. B* **1999**, *103*, 7889−7895.
(22) Lockyer, N. P.; Vickermann, J. C. *Int. J. Mass Spectrom.* **2000**, *197*, 197−209.
(23) Cohen, R.; Brauer, B.; Nir, E.; Grace, L.; de Vries, M. S. *J. Phys. Chem. A* **2000**, *104*, 6351−6355.
(24) Godfrey, P. D.; Brown, R. D. *J. Am. Chem. Soc.* **1995**, *117*, 2019−2023.
(25) McGlone, S. J.; Elmes, P. S.; Brown, R. D.; Godfrey, P. D. *J. Mol. Struct.* **1999**, *485*−*486*, 225−238.
(26) Stepanian, S. G.; Reva, I. D.; Radchenko, E. D.; Rosado, M. T. S.; Duarte, M. L. T. S.; Fausto, R.; Adamowicz, L. *J. Phys. Chem. A* **1998**, *102*, 1041−1054.
(27) Ivanov, A. Yu.; Plokhotnichenko, A. M.; Izvekov, V.; Sheina, G. G.; Blagoi, Yu. P. *J. Mol. Struct.* **1997**, *408*−*409*, 459−462.
(28) Ivanov, A. Yu.; Sheina, G.; Blagoi, Yu. P. *Spectochim. Acta A* **1999**, *55*, 219−228.
(29) Huisken, F.; Werhahn, O.; Ivanov, A. Yu.; Krasnokutski, S. A. *J. Chem. Phys.* **1999**, *111*, 2978−2984.
(30) Jensen, J. H.; Gordon, M. S. *J. Am. Chem. Soc.* **1991**, *113*, 7917−7924.
(31) Godfrey, P. D.; Brown, R. D.; Rodgers, F. M. *J. Mol. Struct.* **1996**, *376*, 65−81.
(32) Chaban, G. M.; Jung, J. O.; Gerber, R. B. *J. Phys. Chem. A* **2000**, *104*, 10035−10044.
(33) Brauer, B.; Chaban, G. M.; Gerber, R. B. *Phys. Chem. Chem. Phys.* **2004**, *6*, 2543−2556.
(34) Depke, G.; Heinrich, N.; Schwarz, H. *Int. J. Mass Spectrom. Ion Processes* **1984**, *62*, 99−117.
(35) Yu, D.; Rauk, A.; Armstrong, D. A. *J. Am. Chem. Soc.* **1995**, *117*, 1789−1796.
(36) Rodríguez-Santiago, L.; Sodupe, M.; Oliva, A.; Bertran, J. *J. Phys. Chem. A* **2000**, *104*, 1256−1261.
(37) Simon, S.; Sodupe, M.; Bertran, J. *J. Phys. Chem. A* **2002**, *106* (23), 5697−5702.
(38) (a) Weiner, P. K.; Kollmann, P. A. *J. Comput. Chem.* **1981**, *2*, 287−303. (b) Weiner, S. J.; Kollmann, P. A.; Case, D. A.; Singh, U. C.; Ghio, C.; Alagona, G.; Profeta, S.; Weiner, P. *J. Am. Chem. Soc.* **1984**, *106*, 765−784.
(39) (a) Jorgensen, W. L.; Tirado-Rives, J. *J. Am. Chem. Soc.* **1988**, *110*, 1657−1666. (b) Jorgensen, W. L.; Maxwell, D. S.; Tirado-Rives, J. *J. Am. Chem. Soc.* **1996**, *118*, 11225−11236.
(40) (a) Halgren, T. A. *J. Comput. Chem.* **1996**, *17*, 490−519. (b) Halgren, T. A. *J. Comput. Chem.* **1996**, *17*, 553−586.
(41) (a) Stewart, J. J. P. *J. Comput. Chem.* **1989**, *10*, 209−220. (b) Stewart, J. J. P. *J. Comput. Chem.* **1989**, *10*, 221−264.
(42) Jensen, F. *Introduction to Computational Chemistry*, Wiley and Sons: Chichester, U.K., 1999; pp 81−92.
(43) Stewart, J. J. P. *J. Mol. Struct. (THEOCHEM)* **1997**, *401*, 195−205.
(44) Lee, T.-S.; York, D. M.; Yang, W. *J. Chem. Phys.* **1996**, *105*, 2744−2750.
(45) Daniels, A. D.; Scuseria, G. E. *J. Chem. Phys.* **1999**, *110*, 1321−1328.
(46) Jung, J. O.; Gerber, R. B. *J. Chem. Phys.* **1996**, *105*, 10332−10348.
(47) Chaban, G. M.; Jung, J. O.; Gerber, R. B. *J. Chem. Phys.* **1999**, *111*, 1823−1829.
(48) http://www.msg.ameslab.gov/GAMESS/GAMESS.html
(49) Stewart, J. J. P.; Davis, L. P.; Burggraf, L. W. *J. Comput. Chem.* **1987**, *8*, 1117−1123.
(50) Maluendes, S. A.; Dupuis, M. *J. Chem. Phys.* **1990**, *93*, 5902−5911.
(51) Taketsugu, T.; Gordon, M. S. *J. Phys. Chem.* **1995**, *99*, 8462−8471.
(52) Taketsugu, T.; Gordon, M. S. *J. Phys. Chem.* **1995**, *99*, 14597−604.
(53) Taketsugu, T.; Gordon, M. S. *J. Chem. Phys.* **1995**, *103*, 10042−10049.
(54) Gordon, M. S.; Chaban, G.; Taketsugu, T. *J. Phys. Chem.* **1996**, *100*, 11512−11525.
(55) Takata, T.; Taketsugu, T.; Hirao, K.; Gordon, M. S. *J. Chem. Phys.* **1998**, *109*, 4281−4289.
(56) Wang, J. P.; Meroueh, S. O.; Wang, Y. F.; Hase, W. L. *Int. J. Mass Spectrom.* **2003**, *230*, 57−64.
(57) Wang, Y. F.; Hase, W. L. *J. Am. Soc. Mass Spectrom.* **2003**, *14*, 1402−1412.
(58) Wigner, E. *Phys. Rev.* **1932**, *40*, 749.
(59) Baer, T.; Hase, W. L. *Unimolecular Reaction Dynamics*; Oxford University Press: Oxford, U.K., 1996.
(60) Schranz, H. W.; Raff, L. M.; Thompson, D. L. *J. Chem. Phys.* **1991**, *95*, 106−120.
(61) Schranz, H. W.; Collins, M. A. *J. Chem. Phys.* **1994**, *101*, 307−321.
(62) Steinfeld, J. I.; Francisco, J. S.; Hase, W. L. *Chemical Kinetics and Dynamics*, 2nd ed.; Prentice Hall: New York, 1998.
(63) Marcus, R. A. *J. Chem. Phys.* **1952**, *20*, 359.
(64) Frost, W. *Theory of Unimolecular Reactions*; Academic Press: New York, 1973.
(65) Gilbert, R. G.; Smith, S. C. *Theory of Unimolecular and Recombination Reactions*; Blackwell: London, 1990.
(66) Holbrook, K. A.; Pilling, M. J.; Robertson, S. H. *Unimolecular Reactions*, 2nd ed.; Wiley and Sons: Chichester, U.K., 1996.
(67) Schranz, H. W.; Raff, L. M.; Thompson, D. L. *J. Chem. Phys.* **1991**, *94* (6), 4219−4229.
(68) Schranz, H. W.; Raff, L. M.; Thompson, D. L. *Chem. Phys. Lett.* **1991**, *182* (5), 455−462.
(69) Sewell, T. D.; Schranz, H. W.; Thompson, D. L.; Raff, L. M. *J. Chem. Phys.* **1991**, *95* (11), 8089−8107.
(70) Schranz, H. W.; Sewell, T. D. *J. Mol. Struc. (THEOCHEM)* **1996**, *368*, 125−131.
(71) Shalashilin, D. V.; Thompson, D. L. *J. Chem. Phys.* **1996**, *105* (5), 1833−1845.
(72) Peña-Gallego, A.; Martínez-Nuñez, E.; Vázquez, S. A. *J. Phys. Chem. A* **1998**, *102*, 8708−8715.
(73) Peña-Gallego, A.; Martínez-Núñez, E.; Vázquez, S. A. *J. Chem. Phys.* **1999**, *110*, 11323−11333.
(74) Martínez-Núñez, E.; Vázquez, S. A. *J. Phys. Chem. A* **1999**, *103*, 9783−9793.
(75) Martínez-Núñez, E.; Vázquez, S. A. *J. Chem. Phys.* **1999**, *111*, 10501−10510.
(76) Martínez-Núñez, E.; Vázquez, S. A. *Theochem-J. Mol. Struc.* **2000**, *505*, 109−116.
(77) Martínez-Núñez, E.; Peña-Gallego, A.; Rodríguez-Fernández, R.; Vázquez, S. A. *Chem. Phys. Lett.* **2000**, *324*, 88−94.
(78) Rahaman, A.; Raff, L. M. *J. Phys. Chem. A* **2001**, *105*, 2147−2155.
(79) Lee, I. R.; Chen, W. K.; Chung, Y. C.; Cheng, P. Y. *J. Phys. Chem. A* **2000**, *104*, 10595−10599.
(80) Peña-Gallego, A.; Martínez-Núñez, E.; Vázquez, S. A. *Phys. Chem. Chem. Phys.* **2000**, *2*, 5393−5399.
(81) Leitner, D. M.; Levine, B.; Quenneville, J.; Martinez, T. J.; Wolynes, P. G. *J. Phys. Chem. A* **2003**, *107*, 10706−10716.